Article:

Al-Kamyani, Z., Figueiredo, F.P., Hu, H. et al. (2 more authors) (2018) Shrinkage and flexural behaviour of free and restrained hybrid steel fibre reinforced concrete. Construction and Building Materials, 189. pp. 1007-1018. ISSN 0950-0618

https://doi.org/10.1016/j.conbuildmat.2018.09.052

Shrinkage and Flexural Behaviour of Free and Restrained Hybrid Steel Fibre Reinforced Concrete

Abstract

The effect of restrained shrinkage on the mechanical performance of concrete and steel fibre reinforced concrete (SFRC) requires more investigation, especially when using recycled tyre steel fibre (RTSF). This paper examines the free and restrained shrinkage strains and the mechanical performance of seven SFRC mixes. Results show that both free and restrained average shrinkage strains are very similar in all blends of fibres and they exhibited non-uniform shrinkage through the height of the section. All examined blends meet strength requirements by MC-2010 for fibres to replace part of the conventional reinforcement in RC structures.

Highlights

- Free shrinkage strains are not affected significantly by addition of steel fibres.
- GGBS reduces shrinkage strains.
- Recycled tyre steel fibres can replace manufactured steel fibres partially.

1. Introduction

In water retaining structures or bridge elements, serviceability limit state (SLS) design aims to control crack widths to achieve a target life span by providing relatively large amounts of surface steel reinforcement. In such structures, the additional reinforcement is required to control cracks induced by restrained shrinkage, which creates further constructability challenges. To reduce the amount of additional surface reinforcement, shrinkage can be mitigated by reducing paste/aggregate ratio, minimising C_3S content in cement, using expansive or shrinkage reducing additives, and internal curing materials [1].

Shrinkage cracking can also be controlled by adding randomly distributed steel fibres as successfully utilised by the construction industry in pavements and tunnels [2, 3, 4]. Steel fibres can enhance the performance of concrete in flexure, shear and punching whilst at the same time help control shrinkage cracking and reduce spalling [5, 6, 7], depending on the amount and characteristics of the steel fibres, such as type, shape and aspect ratio [8, 9, 10, 11]. Recycled tyre steel fibres (RTSF) are also available and were found to be good in controlling micro-cracks [12, 8]. RTSF can improve flexural toughness and post cracking performance and can successfully substitute manufactured fibres partially or fully in some applications [9, 13].

In most published research on RTSF [4, 14, 15], a single type of fibre is used as reinforcement. Recently, some studies investigated blends of manufactured and recycled steel fibres with different shapes and aspect ratios [9, 16], but the recycled fibres used were not classified raising reliability and repeatability concerns. The cleaning process of RTSF has been improved significantly recently and improved classified fibres have become available [17, 18, 19]. Hence, there is a need to investigate the effect of hybrid steel fibres (both manufactured and classified RTSF) on concrete exposed to free and restrained shrinkage.

The impact of steel fibres on free shrinkage of concrete is not clearly understood, with some researchers reporting an increase due to the increase in air voids, whilst others reporting either a decrease due to the internal restraint provided by the fibres or insignificant changes due to the cancelling effect of the two actions [4, 14, 15, 20]. Nonetheless, the effect of steel fibres on free shrinkage is known to vary depending on water-to-binder ratio, volume and type of admixtures, method of concrete laying (conventional, self-compacted concrete (SCC) or roller compacted concrete (RCC)), time of vibration, etc. [21].

In concrete structures, shrinkage of concrete is restrained by different actions internally and externally. External restraint can arise due to friction or reaction against the ground, concrete supporting elements or adjacent rigid structures, whilst internal restraint is provided by aggregates and reinforcement [22, 23]. It is also known that aggregates tend to settle and concentrate at the bottom of the mould whilst water and air rise due to vibration and surface tamping. These phenomena can cause differences in compressive strength and elastic modulus at the top and bottom of the element [24, 25]. As more paste and water are found near the top surface, this can cause much higher shrinkage strains in that region. Non-uniform distribution of aggregates and water can create non-uniform shrinkage through a section and lead to additional curvature in concrete elements [4]. RILEM TC 107-CSP [26] determines shrinkage from the change in the distance between the centres of the two ends of a cylinder, which means that its approach is unable to capture the effect of aggregate sedimentation. To the knowledge of the authors, none of the design codes or standards deal with curvature due to the non-uniform shrinkage and this can lead to underestimate of long-term deflections and crack widths.

Free shrinkage tests on small elements are not normally able to develop enough internal tensile stresses to crack the concrete, hence, restrained shrinkage tests are needed to understand the cracking behaviour of restrained concrete [12]. Restraint causes tensile stresses in the concrete, which theoretically could increase with time due to concrete maturity, but creep is expected to relieve some of these stresses and reduce the probability of cracking [23, 27, 28]. Normally, it is difficult to quantify the degree of restraint imposed on an element, as it depends on the type of application, the location of the member in the structure and environmental conditions [3, 29]. However, there are several tests to assess the restrained shrinkage of concrete [1], with the most used being the ring test [30, 31]. Though simple and popular, this test can only be used for comparison purposes, as it only detects the stress and time of the first crack. Another disadvantage of this approach is that the sectional size needs to be kept relatively small (to enable cracking at a reasonable time frame) and this enhances boundary effects and makes the concrete section less representative of sections in practice.

Active systems with larger specimens [32, 33, 34] can be used to restrain concrete shrinkage by fixing one end of a linear element whilst the other end is attached to an actuator which keeps the total length constant. In active systems, cracks tend to occur when the strain is being adjusted and this can affect the time at which cracking takes place [35]. Furthermore, full and active restrain is rarely found in practice, where restrain depends on the relative stiffness of the restraining structure and is mitigated by creep. For these reasons, and for simplicity, passive systems [36, 37] can be used by restraining concrete specimens through fixing bolts onto rigid structural elements. Younis (2014) [4] proposed the use of a passive restraining frame able to hold three prisms at the same time. The use of linear elements also enables shrinkage measurements to be taken at different levels through the section and examine shrinkage curvature.

The aim of this work is to examine the effect of restrain on shrinkage and mechanical performance of hybrid SFRC mixes. The performance of SFRC prisms comprising different fibre blends and subjected to a combination of restraining, curing and drying conditions are studied and compared. Ground granulated blast-furnace slag (GGBS) and RTSF are used, along with manufactured fibres, to control the amount of shrinkage strains and limit the propagation of concrete cracking under restrained conditions.

This paper comprises three main sections along with an introduction and conclusions. The first section presents the experimental programme including the examined parameters, the physical and mechanical characteristics of the examined materials and testing methodology. This is followed by a discussion on the results obtained from free and restrained shrinkage tests of hybrid SFRC prisms (blends of manufactured undulated steel fibres (MUSF) and RTSF). The level of restrain imposed by restraining frames is assessed through a finite element numerical analysis and used to gain additional insight into the effect of restraint level on overall behaviour. Finally, in the third section the paper discusses the effect of restrained shrinkage and different drying conditions on the flexural performance of the examined concrete mixes.

2. Experimental Programme

2.1 Parameters

The experimental programme examined seven SFRC mixes in addition to a control mix made of plain concrete, as shown in Table 1. Each mix was used to manufacture twelve control cubes (100 mm), six prisms (100x100x500mm) for free shrinkage measurement and three prisms, which were cast in a restraining steel frame as shown in Figure 1a [4]. Three prisms (out of the six) were stored in a mist room (MR) to monitor autogenous shrinkage. The other three specimens were stored under controlled environmental (CR) conditions (temp: 23±2 °C and RH: 40±5%) to quantify drying shrinkage. The restrained specimens (RS) were stored under the same conditions as the CR specimens.

Table 1 Steel fibre types and contents.

Mix	MUSF L (mm)	MUSF Ø (mm)	MUSF Dose (kg/m^3)	RTSF Dose (kg/m^3)	RTPF Dose (kg/m^3)	Batch number
P	-	-	-	-	-	1, 2, 3
M30	55	0.8	30	-	-	1
M20R10	55	0.8	20	10	-	2
M20R10P1	55	0.8	20	10	1	3
R30	-	-	-	30	-	3
M35	60	1.0	35	-	-	1
M45	60	1.0	45	-	-	1
M35R10	60	1.0	35	10	-	2

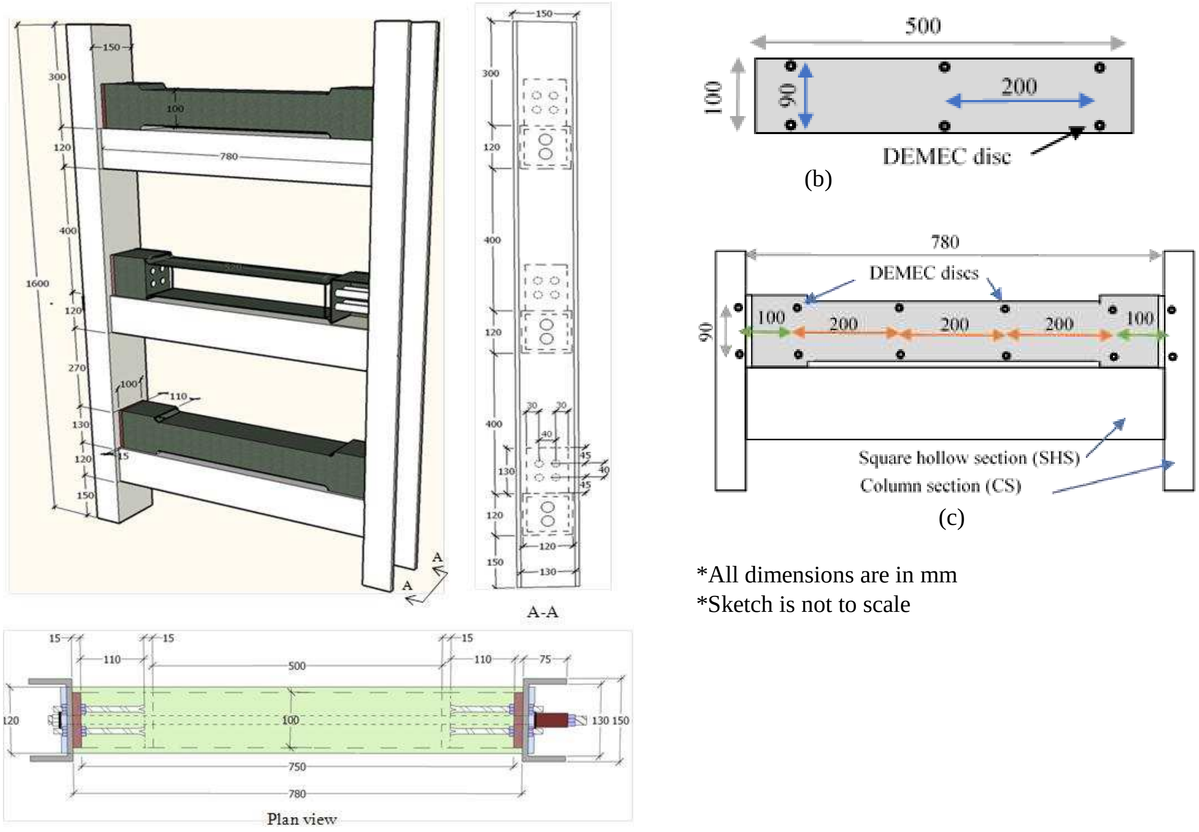

*All dimensions are in mm
*Sketch is not to scale

Figure 1 Restraining frame used to restrain concrete prisms (a) and layout of shrinkage DEMEC distribution in free (b) and restrained prisms (c).

2.2 Measurements

Shrinkage measurements were taken using a 200-mm demountable mechanical “DEMEC” strain gauge at the top and bottom of both sides of all prisms for 300 days. Figure 1 (b and c) shows the measurement layout for free and restrained shrinkage, respectively. It should be noted that a 100 mm “DEMEC” strain gauge was used to measure the deformation at the boundaries between concrete and restraining frame.

At the end of the shrinkage measurement period, CR prisms were dried in an oven until constant weight was observed. This was always achieved after 3 cycles at 50℃ and 3 cycles at 100℃, each cycle lasting 24 hours. After that and prior to flexural testing, all prisms were notched (on one of the sides as cast) at the centre to 1/6 of the sectional depth. They were then tested in three-point flexure by controlling the crack mouth opening displacement

(CMOD) [38]. The exact dimensions of the prisms were taken to the nearest 0.5 mm to account for casting imperfections. Each prism was then split into two pieces and each portion tested for compressive strength according to BS 1881-119 [39]. Concrete compressive strength was also obtained from cube test at 7 days, 28 days and 14 months.

2.3 Materials

Two types of steel fibres were used in this programme: manufactured undulated fibres (MUSF) with a nominal tensile strength of 1450 MPa (two types of undulated length/diameter (L/Ø) 55/0.8 and 60/1) and recycled tyre steel fibres (RTSF) with a nominal tensile strength greater than 2000 MPa [40]. The average diameter of RTSF was about 0.2 mm, whilst the average length, determined using a special optical device, at 50% cumulative mass, was about 20 mm as shown in Figure 2. Both single and blended steel fibres were used to reinforce the concrete in three amounts of 30 kg/m^3, 35 kg/m^3 or 45 kg/m^3. Mix M20R10P1 also contained 1 kg/m^3 of recycled tyre polymer fibres (RTPF) to examine the effect of polymer fibres in controlling shrinkage cracking.

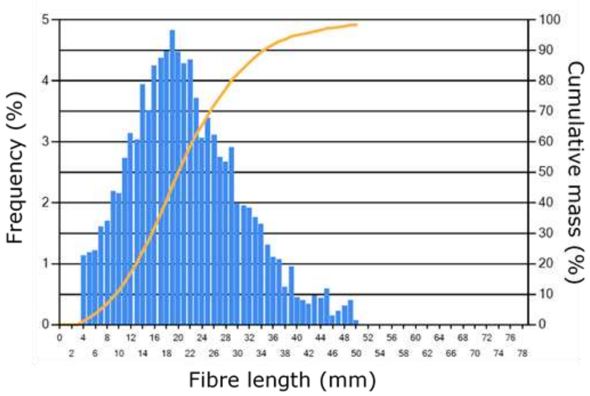

Figure 2 Length distribution of classified RTSF.

Three batches of ready mix concrete were used to manufacture the test specimens (see Table 2). The mix design is based on a design used in Europe for slabs-on-grade. The binder consisted of 50% CEM 1 and 50% GGBS.

Table 2 Nominal mix composition.

Composition	**Quantity (kg/m^3)**
Cement 52.5N CEM1	150
GGBS (BS EN 15167-1:2006)	150
4/20 River aggregates	1097
0/4 River sand	804
Water/binder ratio	0.55
SP (Master Polyheed 410)	1.5 L

3. Results and Discussion on Shrinkage Strains

3.1 Free shrinkage strains

3.1.1 Drying shrinkage

The free shrinkage strains versus time at the top and bottom of the specimen (T for top and B for bottom) are shown in Figure 3 (a and b), respectively. The small fluctuations in the curves are a result of small temperature and relative humidity changes in the control room. Shrinkage strain predictions of Eurocode [41] and fib Model Code [42], shown in dotted lines, are higher than the experimental strains, possibly due to the high amount of GGBS and differences in first measurement time. The EC and fib models consider conventional cements and do not consider other cementitious materials in their predictions. GGBS was found by some authors to reduce total shrinkage amount (average of top and bottom measurement) [35, 43, 44] as the fineness of GGBS can close the concrete pores and prevent water from escaping the substrate [27]. Codes recommend taking the first shrinkage measurements within 3 minutes after demoulding, but due to the high amount of DEMEC discs used in this study, the first shrinkage measurement was taken after 6 hours.

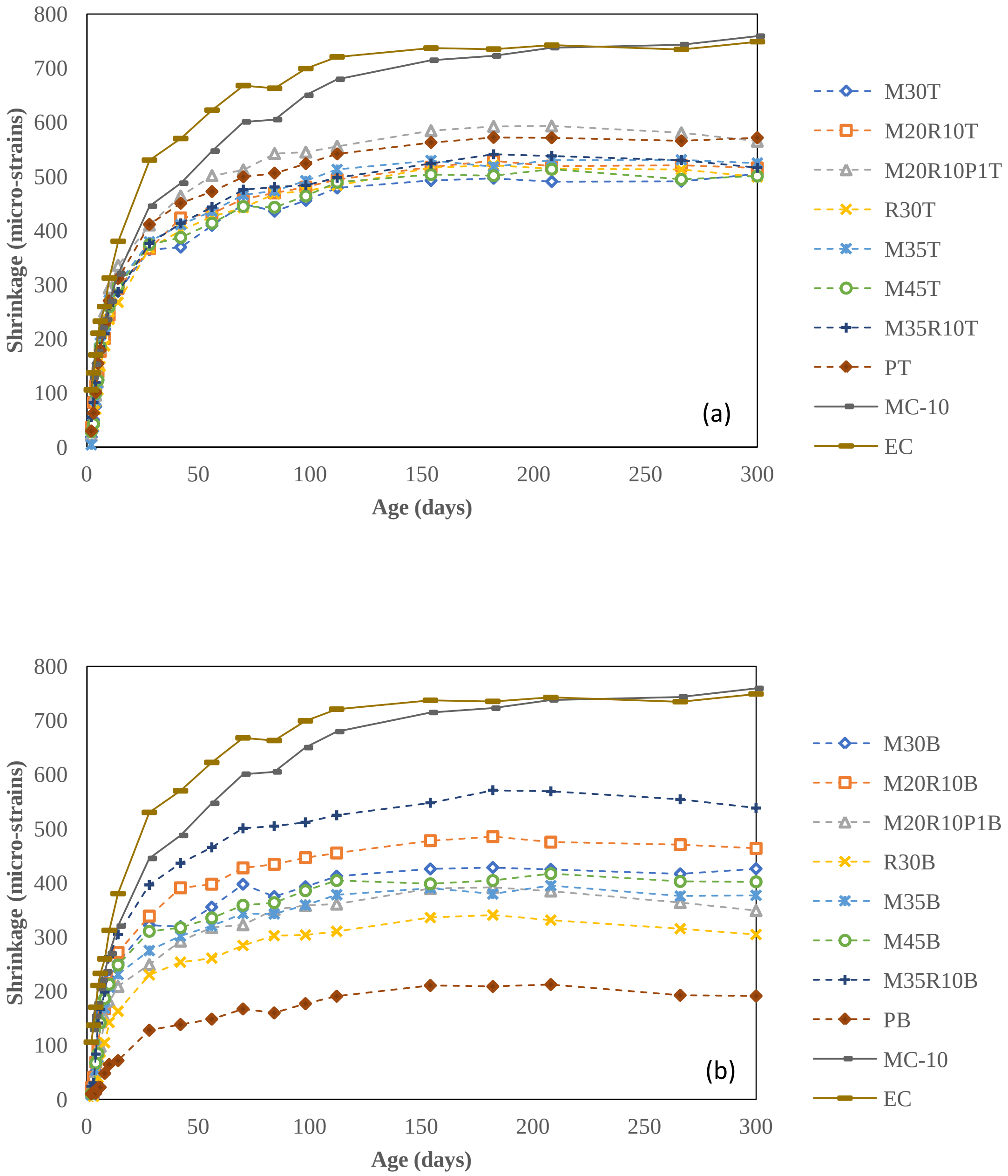

Figure 3 Free shrinkage strains at top (a) and bottom (b).

It is difficult to determine, from the results, the precise effect of steel fibre type/dosage on free shrinkage. However, it is evident that shrinkage strains at the top are overall higher than at the bottom possibly due to non-uniform distribution of concrete constituents. Plain concrete shows higher shrinkage strains at the top than SFRC mixes, whilst showing the lowest strain at the bottom. This may be due to the fact that superplasticiser was added to the plain concrete (to maintain the workability of concrete after the addition of steel fibres) and this may have led to more bleeding than in the other mixes. Overall, SFRC specimens experienced higher amounts of average shrinkage strains compared to plain concrete, possibly due to the air entrainment on the surface of the fibres. Shrinkage strains of SFRC were between 500 and 600 micro-strains at the top and between 300 and 500 micro-strains at the bottom. The scatter of the bottom measurements was higher than that of the top measurements possibly due to the fact that the presence of steel fibres prevented some of the coarse aggregates from settling to the bottom of the mould [45]. The varying amounts of coarse aggregates at the bottom of the section resulted in varying degrees of restrain and thus a higher scatter in shrinkage resistance. Non-uniform shrinkage strains in these rectangular sections can be the result of non-uniform distribution of the coarse aggregates across the depth of concrete section, which also creates curvature that will contribute to the global deformation of the members [25, 45].

3.1.2 Drying shrinkage and mass loss relationship

The relationship between total free shrinkage and mass loss of the CR specimens is shown in Figure 4. Though the water content in the original mix was the same for all mixes, workability decreased after introducing steel fibres as some of the free water was adsorbed in wetting the surface of the fibres. Hence, it appears that, as a result, the plain concrete mix lost more free water than the SFRC mixes during the first few days of drying.

The behaviour of each mix shows three stages: 1) the first five days of rapid drying, 2) normal drying and 3) accelerated drying in the oven. The first stage indicates rapid mass loss possibly due to the evaporation of the free water [46]. The second stage tends to show a linear trend in mass loss with free shrinkage until mass loss stabilises and the moisture inside the samples become approximately equal to the relative humidity of the atmosphere [36]. The third stage was created artificially due to accelerated drying of the prisms in the oven initially at 50 °C and then at 100 °C. During the first three cycles at 50 °C, there was little change in mass loss and shrinkage. However, once the temperature was elevated to 100 °C, there was a noticeable increase in mass loss and drying shrinkage.

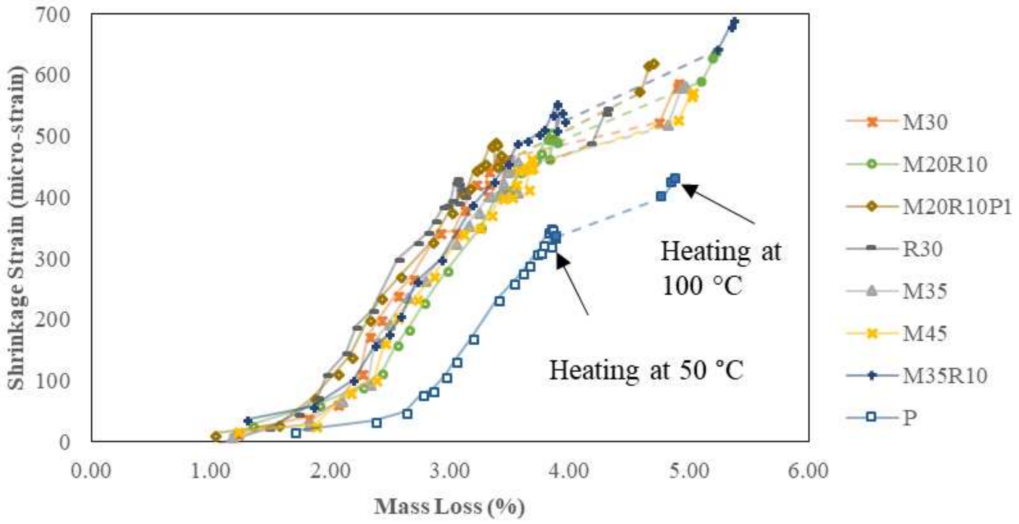

Figure 4 Free shrinkage and mass loss relationship.

The purpose of completely drying the samples was to assess if it is possible to predict the ultimate drying shrinkage strains from mass loss by assuming that the relationship between shrinkage and mass loss is linear. However, during accelerated drying, there was more mass loss (on average 14%) or less shrinkage (on average 19%) than expected under normal drying conditions (second stage). This phenomenon may be attributed partly to micro diffusion of water from gel pores to capillary pores, which helps to free larger amounts of water [47], or to the micro-cracking that was caused by differential temperature at the surface of the concrete during cooling. This was evident in the plain concrete that showed the highest number of micro-cracks on the surface. Therefore, heating the samples at 100 °C appears to have altered the mechanism of drying due to micro diffusion of water or micro-cracking, which was not intended by the experiment. However, the ultimate mass loss could be obtained at lower temperatures, e.g. at about 80 °C without causing damage in the concrete micro-structure, and could be used to predict the long-term evolution of drying shrinkage strain and its impact on the health of the structure.

3.1.3 Humid concrete shrinkage strains

Figure 5 shows the evolution of shrinkage strain in specimens conditioned in a mist room. Negative strain values mean that the samples are swelling. The non-uniformity in the curves between age of 50 and 70 days was due to unexpected fluctuations in moisture inside the mist room (due to some mechanical problems). The initial swelling in the samples can be attributed to swelling in GGBS grains, which can absorb water and lead to disjointing pressure [48, 49], as they get fully saturated during the hydration process. As a result, swelling continues until the relative humidity in the matrix becomes less than the relative humidity in the pores of the grains [50]. However, the plain concrete specimens swelled less compared to those reinforced with fibres, possibly due to their lower permeability, which prevented the GGBS in the matrix from absorbing any additional water [51].

Swelling continued for the entire 11-month period of measurements, which indicates that swelling due to absorption of moisture is higher than any autogenous shrinkage strains. Model B3 [47] and fib MC-2010 [42] predict expansion in any concrete stored under relative humidity of about 100%. Predictions by model B3 and fib MC-2010 are shown in dashed lines in Figure 5 (indicated as B3 and MC, respectively). B3 is found to be in agreement with the initial experimental results while MC is close to the plain concrete throughout the measuring period. It should be noted that this analysis was carried out using CEM I as a cementitious material in both models as there is no provision for GGBS in the current formulations. fib MC-2010 was found to predict expansion strains up to two times greater than those induced by autogenous shrinkage strains.

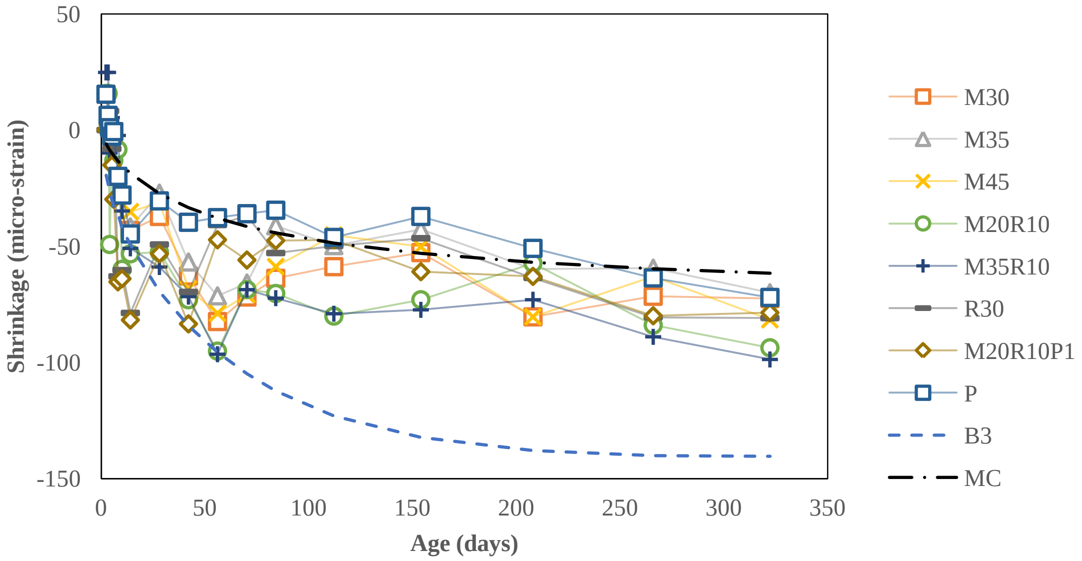

Figure 5 Humid concrete strain results.

3.2 Restrained shrinkage strains

Figure 6 (a and b) shows the restrained shrinkage strains of all tested prism at the top (T) and bottom (B), respectively. In general, prisms made with different mixes exhibited similar restrained shrinkage strain development, apart from those made with mixes M35 and R30, which started deviating from the rest between the age of 14 and 28 days. No significant development in shrinkage took place in mix M35, possibly due to early age micro-cracking near the anchors, whilst there was a remarkable increase in mix R30, possibly due to slip at the interface between concrete and anchors.

Shrinkage strains varied between 250 and 300 micro-strains at the top and between 160 and 180 micro-strains at the bottom at the age of 180 days. These strains decreased after 200 days, possibly as a result of creep and the development of micro-cracks inside the concrete. The similarity in the shrinkage strain levels exhibited by all specimens indicates that the effect of steel fibre type and dosage is insignificant with respect to restrained shrinkage, as was also observed in free shrinkage prisms. It should be noted that some of the curvature induced in the specimens can be attributed to restraint loss at the external boundaries between the concrete and steel anchors and/or differential aggregate distribution.

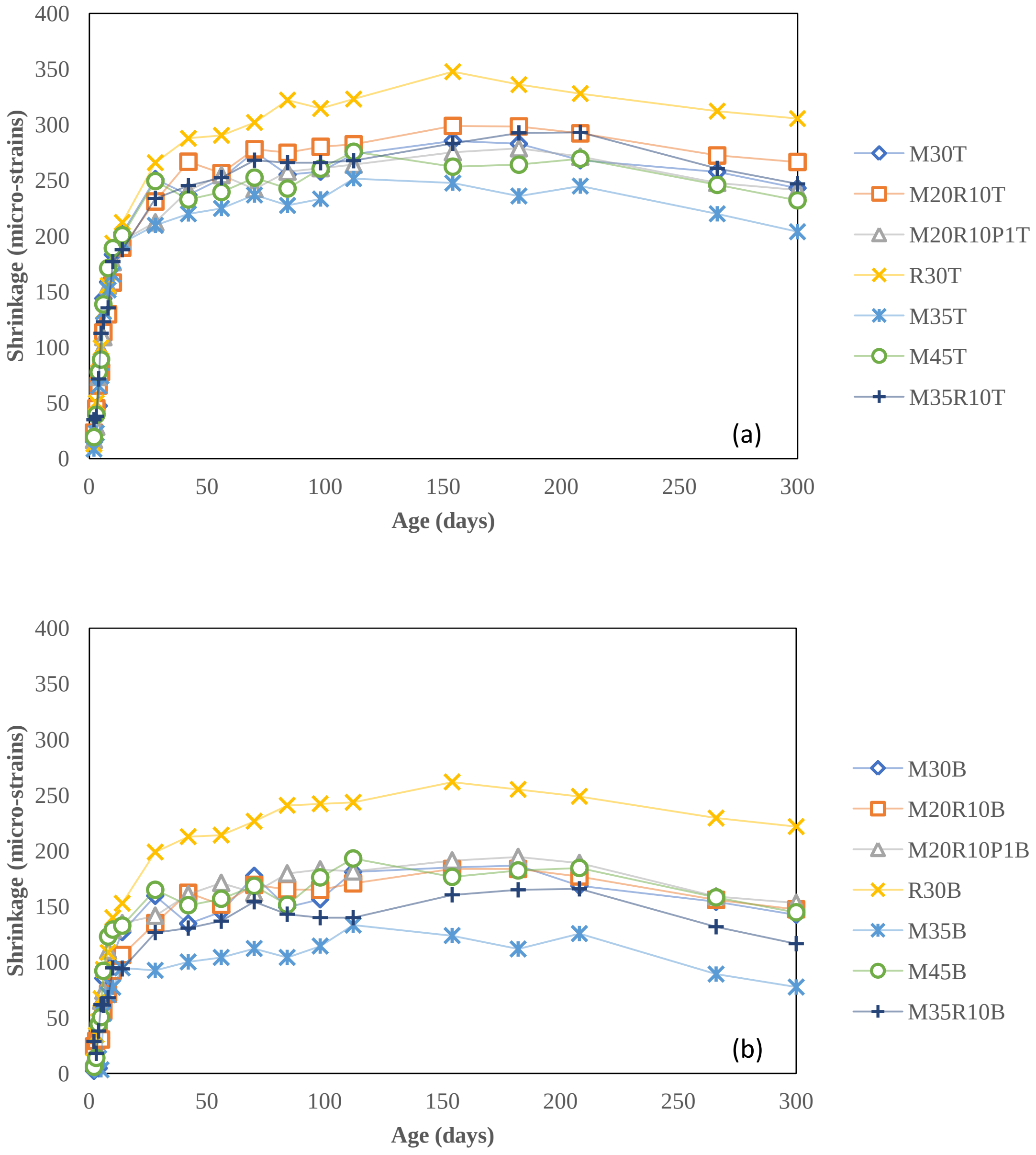

Figure 6 Restrained shrinkage strains at top (a) and bottom (b).

3.3 Performance of the restraining frame

The degree of restraint (DOR) is defined as the difference in strain between the free and restrained elements (see Equation (1)). The DOR values for the passive restraining frame used varied between 0.5 and 0.6. The theoretical values using simple elastic calculations is higher at 0.73 [12].

$$DOR = \frac{\varepsilon_{sh,free} - \varepsilon_{sh,restrained}}{\varepsilon_{sh,free}} \qquad (1)$$

Drying shrinkage induces shortening of the concrete specimens, which are restrained by the frame through the anchors. Figure 7 shows that there is some additional deformation at the boundaries between concrete and the restraining frame over a gauge length of 100 mm (see Figure 1c) for a typical mix (M20R10P1) at the top (T) and bottom (B) of each specimen (1 - top, 2 - middle and 3 - bottom prism in the restraining frame). The deformations are higher at the top of prisms 2 and 3 whilst they are similar for all prisms at the bottom level. Most of the deformation takes place during the first 50 days. This deformation is the result of: a) elastic deformation of the concrete, b) anchor elongation, c) slip at the interface between concrete and anchors and d) local deformation of the frame. These additional deformations b), c) and d) contribute to the differences between the actual (0.57) and theoretical (0.73) DOR.

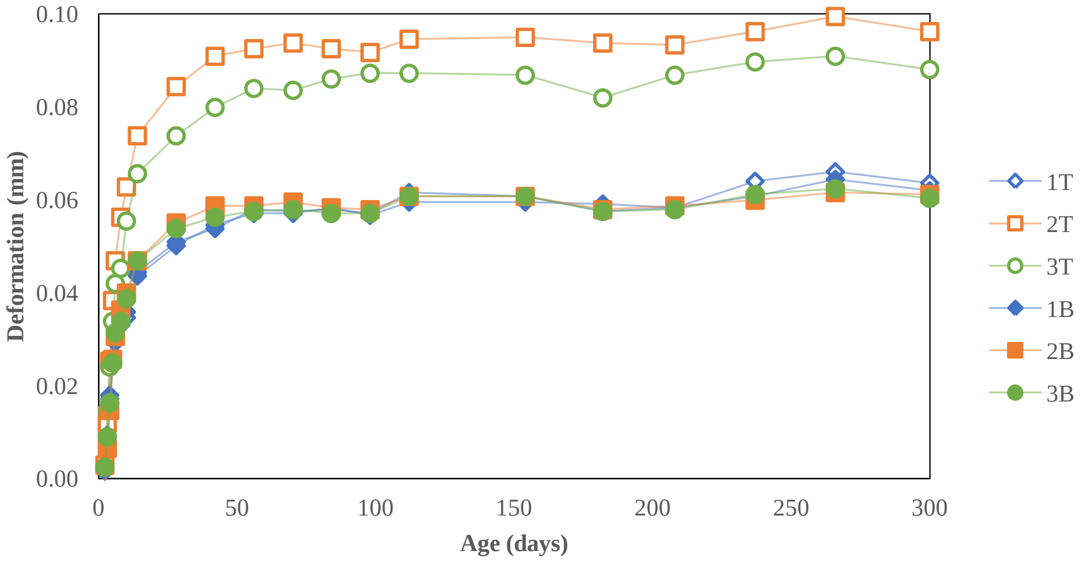

Figure 7 Deformation at the boundary between restraining frame and concrete specimens, mix M20R10P1.

A numerical investigation was conducted by Younis (2014) [4] using 3D linear FEA models in ABAQUS [52] to estimate the induced deformations by concrete drying shrinkage on the restraining frame. Solid (continuum) elements with 8 integration points (CD8R) were used. The approximate global mesh size was 20 mm, but a finer mesh was adopted close to the connections. The model was run without the presence of concrete elements and pre-stressing forces on the rods inside the square hollow sections (SHS). This study adopted this model, but modified the boundary conditions, modelling of concrete prisms and pre-stressed forces as follows; the right column (CS) was fixed (welded) to the SHSs and to the base of the frame whilst the left CS was pinned by pre-stressed forces of 56.25 kN (the result of a torque of 180 N.m on the bolts) applied to rods inside the SHS. The anticipated induced force due to drying shrinkage ($\varepsilon_{sh}E_cA_c$), at the age of 300 days, was applied uniformly on the anchors. At this age, the specimens have reached hygral stabilisation and the relative deformation between concrete and frame can be considered to be approximately stabilised (see Figure 7). Therefore, the shrinkage induced force can be assumed to be 100% resisted by the anchors.

Figure 8 shows the exaggerated global and local deformations of the restraining frame obtained by FEA. Concrete shrinkage caused relative translation of the CS and bending in both CS and SHS. The relative translation between the columns at the level of prism 1, 2 and 3 is 0.127, 0.075 and 0.087 mm, respectively, corresponding to RF of 0.64, 0.79 and 0.75. The bending deformation of the SHS restraining prism 1 is higher than that at prisms 2 and 3 due to the free end effect. Prism 2 experienced the lowest deformations due to the restraint contribution of both top and bottom SHSs. Figure 8b shows the local deformation of the CS at the level of prism 2 and the relative deformation between web and flanges. This highlights the additional contribution to the boundary zone deformation due to local deformations of the frame, which can actually account for some of the deformation shown in Figure 7. Much of this local deformation can be avoided if the CS is locally stiffened to prevent the flange rotation. The average apparent measured RF at 300 days was 0.57 whilst the theoretical and numerical DORs are very similar at 0.73.

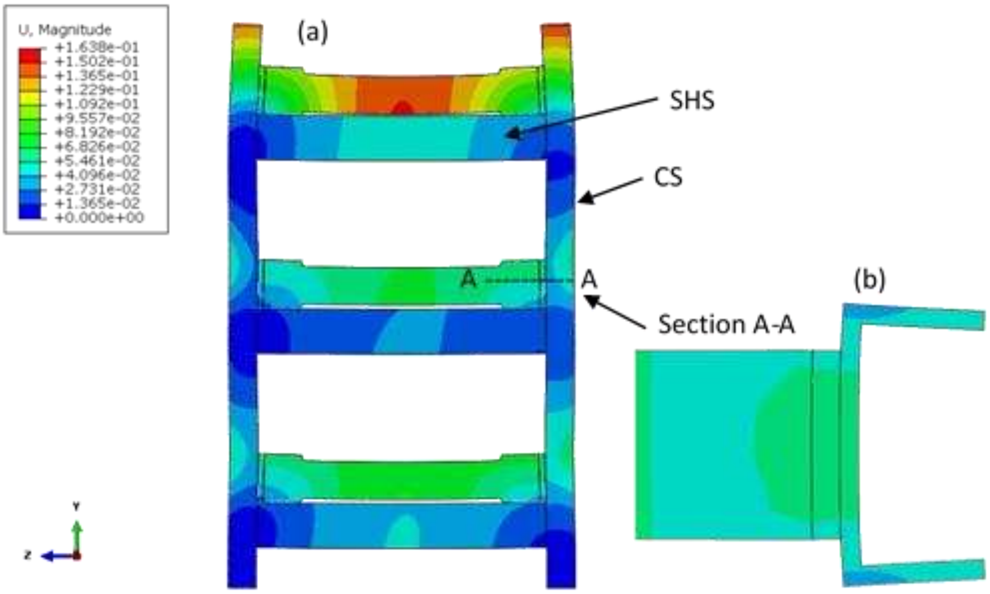

Figure 8 Exaggerated global and local deformation in the restraining frame (a) and supporting column (b).

4. Results and Discussion on Mechanical Characteristics

4.1 Compressive strength

Table 3 shows the average results of density and compressive strength for the plain concrete mixes, for both air and water cured cubes (standard deviations are shown in parenthesis). For air cured cubes, there was only a slight increase in the compressive strength between 7 and 28 days whereas for water cured specimens, there was a dramatic change in compressive strength due to the activation of the GGBS in the presence of water. The GGBS is also responsible for the lower in early strength of the water cured samples at 7 days [35, 53]. At 14 months, the compressive strength for the samples stored in air is similar to that measured at 28 days, while there was an increase from 40 MPa to 56 MPa for the water cured samples.

Table 3 Plain concrete density and compressive strength results (standard deviation).

Curing	**Density (kg/m^3)**			**Compressive Strength (MPa)**		
method	**7 days**	**28 days**	**14 months**	**7 days**	**28 days**	**14 months**
Air cured	2310 (34)	2285 (11)	2284 (42)	20.7 (0.2)	24.5 (1.6)	24.1 (0.3)

Water Cured	2387 (11)	2415 (16)	2405 (29)	22.6 (0.6)	40.1 (0.2)	56.0 (1.2)

Figure 9 shows the mean compressive strength values, obtained from three cubes (150 mm) per mix at 35 and 105 days (moisture cured in the laboratory) as well as from six samples for each curing condition (MR, CR, RS) obtained from the broken prisms in flexure at the age of 14 months. At age of 14 months, SFRC obtained from broken prisms shows higher compressive strength compared to plain concrete at the same curing condition. However, in all cases, the dose of the steel fibres appears to have no clear effect on compressive strength.

As expected, prisms stored in the mist room (MR) show much higher compressive strength compared to the ones air cured in the control room (CR and RS) by about 56% on average. CR and RS samples resulted in similar compressive strengths despite the fact that RS samples were restrained for ten months and experienced drying shrinkage micro-cracks. This may be because CR samples were fully dried in an oven (to determine mass loss) which may have caused micro-cracks and weakened their structure. Micro-cracks were observed on the surface of plain concrete specimens as discussed in subsection 3.1.2.

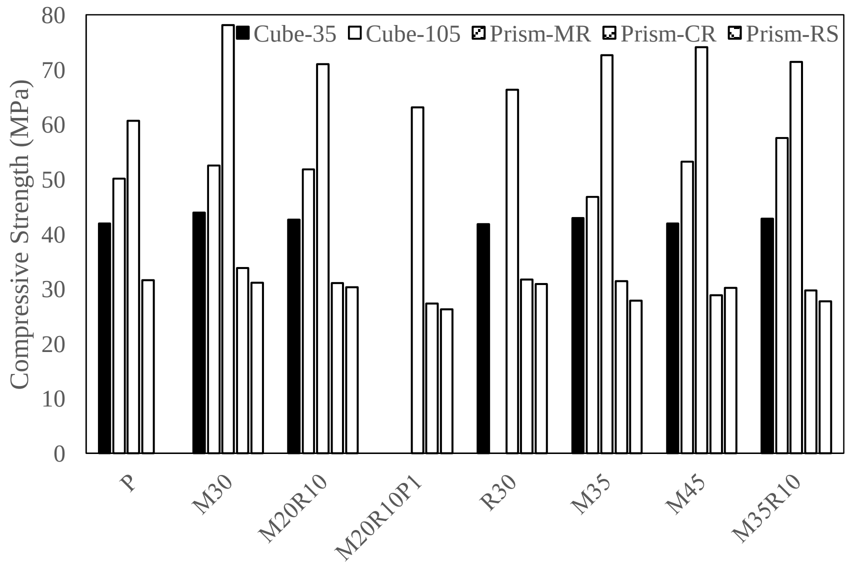

Figure 9 Compressive strength obtained from cubes at 35 and 105 days and broken prisms in flexure at 14 months.

4.2 Flexural Performance

Figure 10 (a-f) shows the stress-CMOD results (average of three prisms) for specimens conditioned in MR, CR and RS environments. The initial elastic behaviour of all specimens, shown in the graphs up to CMOD of 0.2 mm, is very similar. This confirms that the test arrangement and measuring method is accurate and reliable and that the fibre content does not influence much the elastic modulus. The plain concrete mix (P) shows the lowest strength and least overall toughness. The fibre content seems to have some influences on residual tensile strength with some mixes (e.g. CR M35) showing up to 100% increase in strength and clear strain hardening characteristics. The initiation of cracking in the plain concrete appears to take place just before the peak load at a CMOD of 0.02 mm. The same applies to all other specimens and, as expected, fibres get mobilised and control the crack development. In several cases, there is some initial drop in stress after the opening of the crack at around 0.03 mm until the fibres are mobilised sufficiently and contribute to stiffening the cracked concrete. Sudden drops in stress are also seen in the post-peak range, due to fibre fracture or slip.

All prisms conditioned in the mist room (MR) show higher strength and toughness than the CR specimens by about 40% on average. This highlights the importance of curing in strength development as well as the dominance of concrete strength on the flexural strength of SFRC. Higher concrete strength also results into higher bond strength between the concrete and fibres, which contributes to higher toughness. However, this also leads to more fibres fracturing during the post-peak stage than slipping, as indicated by the fracturing sounds during the test. In the case of the MR conditioned specimens (see Figure 10b), the higher concrete strength leads to a high flexural strength when the first crack develops, but due to high bond, more fibres break, leading to mainly flat post-cracking behaviour. On the other hand, CR and RS conditioned specimens, which have a lower concrete strength, show a lower flexural strength at first crack, but mobilize more fibres due to slippage, which leads to smoother curves with hardening behaviour [54, 55].

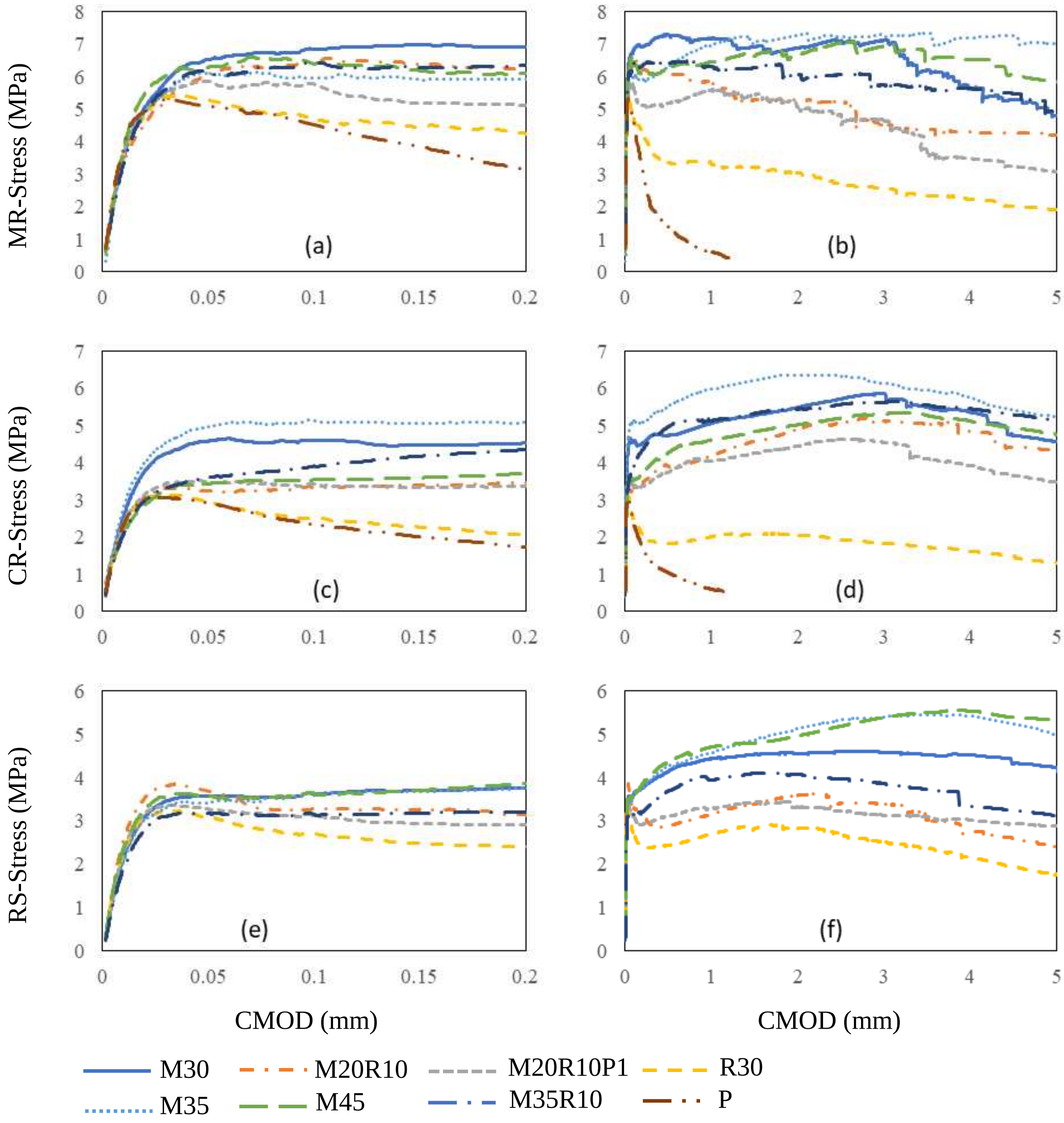

Figure 10 Stress-CMOD curves a) MR-0.2 mm, b) MR, c) CR-0.2 mm, d) CR e) RS-0.2 mm, f) RS.

4.3 Residual flexural tensile strength

This sub-section examines the effect of fibre type and dosage, curing and restrain condition on the flexural strength at the limit of proportionality (f_{LOP}) and residual flexural tensile strength values (f_{R1}, f_{R2}, f_{R3}, f_{R4}) at different CMODs (0.5 mm, 1.5 mm, 2.5 mm and 3.5 mm). In accordance to EN 14651:2005, f_{LOP} is taken as the maximum stress value up to CMOD of 0.05 mm.

4.3.1 Effect of curing

Figure 11 (a and b) shows the change in flexural strength and residual values for the specimens subjected to different conditions (MR and RS) relative to the CR condition. Figure 11a shows that mist curing increases f_{LOP} by up to 90% (on average 60%), but this increase decreases at larger CMODs. This confirms that curing has a significant effect on concrete strength development as reflected by the increase in f_{LOP}. However, as the effect on f_R values reduces with increasing CMOD, curing condition has less impact on the bridging capacity of fibres which, at large CMOD, depends more on frictional stresses, geometrical characteristics and less on bond strength.

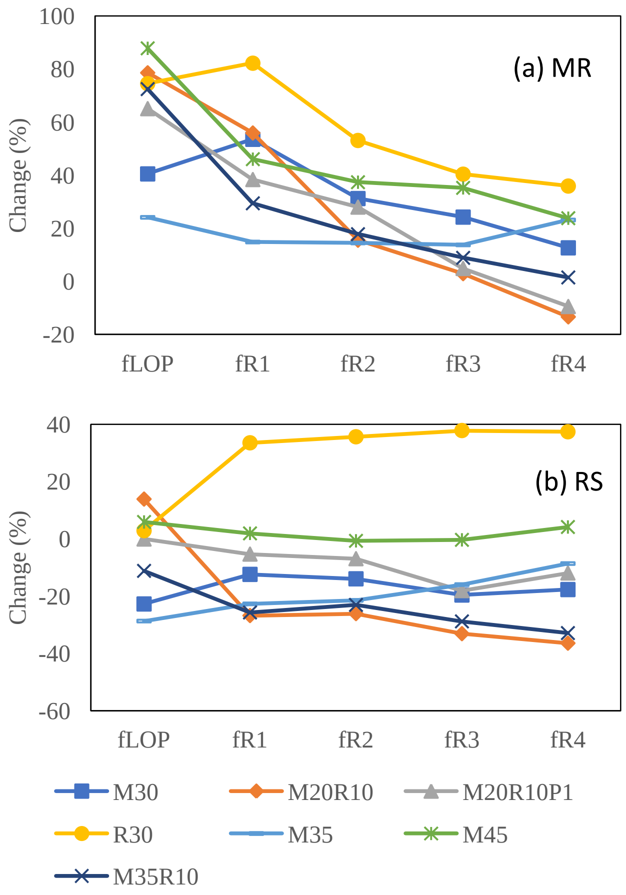

Figure 11 Change in flexural and residual flexural tensile strength relative to CR in a) MR and b) RS.

4.3.2 Effect of restraint

Figure 11b shows the relative change in flexural strength due to restraint. The figure shows an overall loss of f_{LOP} on average of 10% due to restraint, despite the fact that no cracks were visible on the RS specimens. However, as tensile strain and stress developed in the RS specimens, micro-cracking must have taken place and caused some damage to the concrete. The effect of the damage and micro-cracks appears to overall increase marginally as the CMOD increases. Specimens manufactured with mix R30 show better performance partly because they were not well restrained, thus could lead to smaller cracks that self-healed. Self-healing in restrained concrete was also reported by Younis (2014) [4].

4.3.3 Effect of fibres

Figure 12 (a-c) shows the change in flexural strength and residual flexural tensile stresses due to the substitution of MUSF with RTSF for a total fibre content of 30 kg/m^3 under MR, CR and RS conditions, respectively. The changes are shown relative to M30 for each respective condition. In Figure 12a, the effect of substituting MUSF with 10 kg/m^3 of RTSF results in about 10% reduction in both f_{LOP} and residual flexural tensile stresses, as this substitution did not affect much the concrete tensile strength and concrete-fibre interface bond strength. In larger specimens (150 mm prisms and slabs), the blends with 10 kg/m^3 RTSF showed a positive change in f_{LOP} and f_R values [40]. This can be attributed to the fact that fibre alignment is more critical in cast elements with small cross section due to boundary effect, thus a small reduction in the amount of MUSF (which is longer) can affect significantly the post cracking behaviour. The highest strength reduction at bigger CMODs was observed in specimens made with mix R30, partly due to fibre slippage as RTSF have shorter and thinner geometries compared to MUSF and partly due to their more random distribution. The reduction in f_{LOP} for specimens conditioned in CR (Figure 12b) is higher than that found in MR samples by about 20%, but this may be more to do with the high f_{LOP} values of M30 than the effect of fibres, as the f_R values changes are similar to those observed for MR samples (Figure 12a).

When the concrete is restrained (see Figure 12c), even though there is an overall drop in f_{LOP} of 10%, the fibres do not appear to influence f_{LOP}. However, there is a drop of about 30% in the f_R values of the blended mixes and of about 40% for the R30 mix. This is possibly due to the reasons given above to Figure 12a.

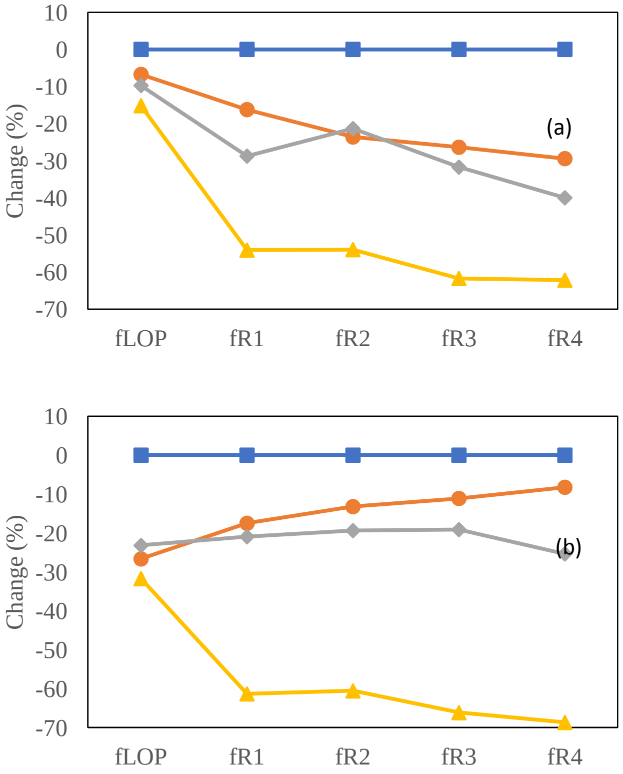

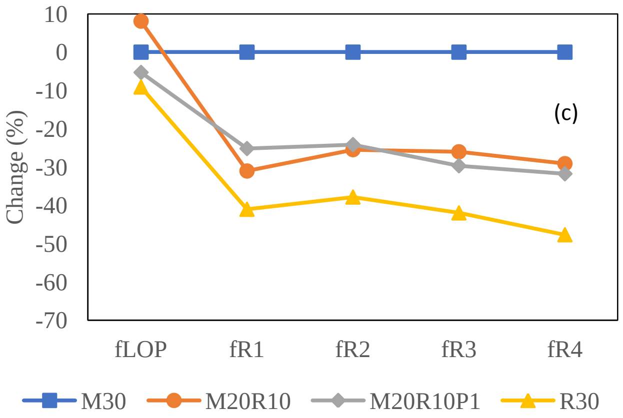

Figure 12 Change in residual flexural tensile strength due to substitution of MUSF with RTSF conditioned in a) MR, b) CR and c) RS.

4.4 Characteristic residual flexural tensile strength ratios

In order to replace parts of conventional reinforcement with fibres in concrete structures, fib MC-2010 imposes that the minimum values of characteristic residual flexural tensile strength ratios at serviceability (f_{R1k}/f_{Lk}) and ultimate limit state (f_{R3k}/f_{R1k}) conditions, be 0.4 and 0.5, respectively (f_{Lk}, f_{R1k} and f_{R3k} are the characteristic values at f_{LOP}, f_{R1} and f_{R3}, respectively). These characteristic values are calculated using RILEM TC 162-TDF (2003) [56] and depend on the number of specimens tested per parameter.

Figure 13 shows the serviceability characteristic residual flexural tensile strength ratios (f_{R1k}/f_{Lk}) for all mixes in MR, CR and RS conditions. Mixes with a total of 30 kg/m^3 of steel fibres show ratios less than one, while mixes with a total of 45 kg/m^3 show ratios mostly greater than one. Mixes with 45 kg/m^3 contain considerably more longer manufactured fibres which have a larger diameter and can resist tension more effectively even at larger CMOD. CR and RS specimens with a total fibre content more than 35 kg/m^3 have higher ratios than MR specimens, due to their lower f_{LOP}.

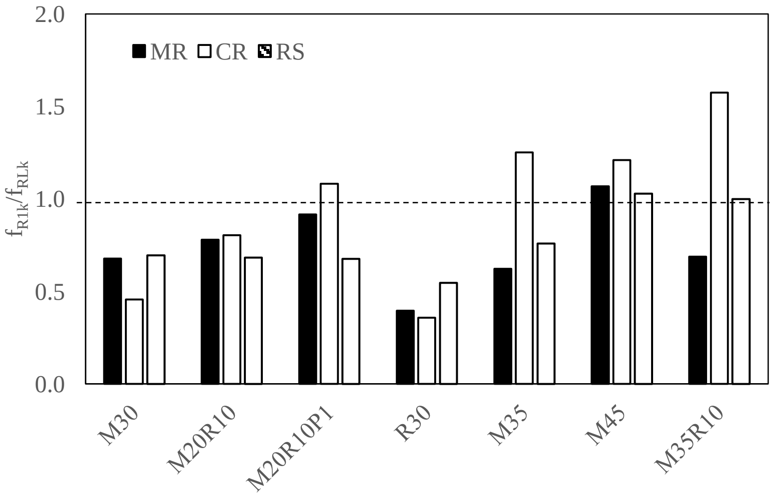

Figure 13 Ratio of characteristic strength, fR1k/fLk.

Figure 14 shows the ultimate characteristic residual flexural tensile strength ratios (f_{R3k}/f_{R1k}) for all specimens subjected to MR, CR and RS conditions. Most of f_{R3k}/f_{R1k} ratios for the CR and RS specimens are greater than those for MR samples. This can again be attributed to the higher f_{LOP} achieved in the MR samples as a result of better curing. Overall, all blends satisfied the required ratios of fib MC-2010 for serviceability and ultimate limit states. Hence, blends of MUSF and RTSF can be used to replace part of conventional reinforcement in RC structures.

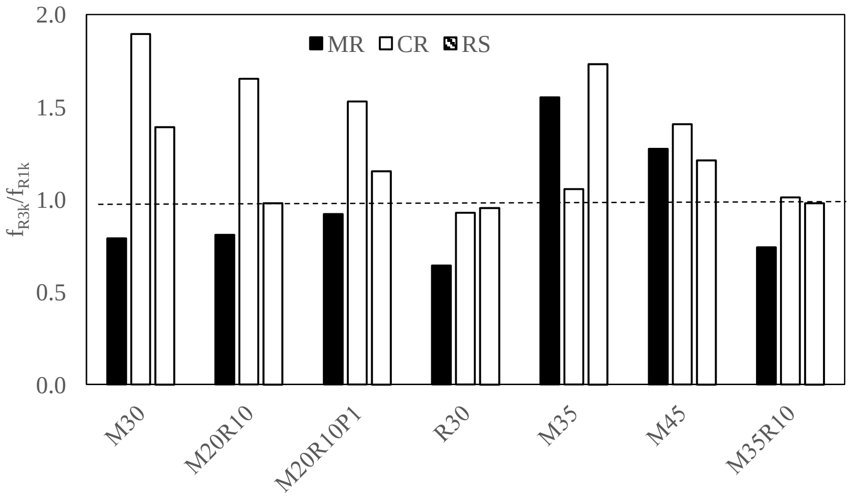

Figure 14 Ratio of residual characteristic strength, fR3k/fR1k.

5. Conclusions

This paper presents the free and restrained shrinkage behaviour of FRC specimens with different fibre type (MUSF, RTSF and various blends) and their associated mechanical characteristics. It has been shown that the utilisation of GGBS and RTSF in concrete mixes contributes to reducing shrinkage strains and controlling cracking. Based on the experimental results the following conclusions can be drawn:

- Free shrinkage was much lower than predicted by the design codes by 35% on average due to the use of GGBS.
- Non-uniform shrinkage strains through the height of plain and SFRC sections were observed in free and restrained elements, possibly due to uneven distribution of coarse aggregates.
- Average shrinkage strains in SFRC were higher than in plain concrete, possibly due to an increase in air voids.
- Drying and end restraint caused the development of micro-cracking in the concrete which resulted in lower compressive strength (by about 56% on average) and residual flexural tensile strength (up to 40%).
- Curing has a significant effect on concrete strength development, but less impact on the bridging capacity of fibres which depends more on frictional stresses.
- The high residual flexural tensile strength of SFRC (cured in MR) and the high frictional stresses between the concrete and the fibres caused the used small dosages of fibres to break, due to the highly applied tensile stress on fibres.
- The decay in the stress-CMOD curves show that the hybrid mixes of MUSF and RTSF satisfy the ratios imposed by the fib MC-2010 and can reduce the required amount of conventional reinforcement in concrete structures.

Acknowledgments

The researchers are gratefully acknowledging the financial support provided by the EC collaborative FP7-ENV-2013-two-stage project "ANAGENNISI - Innovative Reuse of All Tyre Components in Concrete" under grant number 603722 and the Omani government for sponsoring the first author. We also appreciate the technical support provided by the postgraduate students and engineering technicians in the concrete laboratory.

References

[1] ACI-231R, “Report on Early-Age Cracking: Causes, Measurement, and Mitigation,” American Concrete Institute, Farmington Hills, 2010.

[2] N. Buratti, B. Ferracuti and M. Savoia, “Concrete crack reduction in tunnel linings by steel fibre-reinforced concretes,” *Construction and Building Materials,* vol. 44, p. 249–259, 2013.

[3] N. Banthia, C. Yan and S. Mindess, “Restrained Shrinkage Cracking in Fiber Reinforced Concrete: A Novel Test Technique,” *Cement and Concrete Research,* vol. 26, no. 1, pp. 9-14, 1996.

[4] K. H. Younis, “Restrained shrinkage behaviour of concrete with recycled materials,” The University of Sheffield, Sheffield, 2014.

[5] Z. Zamanzadeh, L. Lourenço and J. Barros, “Recycled Steel Fibre Reinforced Concrete failing in bending and in shear,” *Construction and Building Materials,* vol. 85, p. 195–207, 2015.

[6] D.-Y. Yoo, Y.-S. Yoon and N. Banthia, “Predicting the post-cracking behavior of normal- and high-strength steel-fiber-reinforced concrete beams,” *Construction and Building Materials,* vol. 93, p. 477–485, 2015.

[7] M. Bartolac, D. Damjanović, J. Krolo, I. Duvnjak and A. Baričević, “Punching of slabs reinforced with recycled steel fibres from used tyres,” Dundee, 2016.

[8] A. Kaïkea, D. Achoura, F. Duplan and L. Rizzuti, “Effect of mineral admixtures and steel fiber volume contents on the behavior of high performance fiber reinforced concrete,” *Materials and Design,* vol. 63, p. 493–499, 2014.

[9] E. Martinelli, A. Caggiano and H. Xargay, “An experimental study on the post-cracking behaviour of Hybrid Industrial/Recycled Steel Fibre-Reinforced Concrete,” *Construction and Building Materials,* vol. 94, p. 290–298, 2015.

[10] S. Yazıcı, G. Inan and V. Tabak, “Effect of aspect ratio and volume fraction of steel fiber on the mechanical properties of SFRC,” *Construction and Building Materials,* vol. 21, p. 1250–1253, 2007.

[11] G. Chanvillard and P.-C. A'itcin, “Pull-Out Behavior of Corrugated Steel Fibres,” *Advn Cem Bas Mat,* vol. 4, pp. 28-41, 1996.

[12] K. H. Younis and K. Pilakoutas, “Assessment of Post-Restrained Shrinkage Mechanical Properties of Concrete,” *ACI MATERIALS JOURNAL,* vol. 113, no. 3, pp. 267-276, 2016.

[13] G. Centonze, M. Leone and M. Aiello, “Steel fibers from waste tires as reinforcement in concrete: A mechanical characterization,” *Construction and Building Materials,* vol. 36, pp. 46-57, 2012.

[14] N. Jafarifar, “Shrinkage Behaviour of Steel Fibre Reinforced Concrete Pavements,” The University of Sheffield, Sheffield, 2012.

[15] Â. G. Graeff, “Long-term performance of recycled steel fibre reinforced concrete for pavement applications,” The University of Sheffield, Sheffield, 2011.

[16] B. Akcay and M. A. Tasdemir, “Mechanical behaviour and fibre dispersion of hybrid steel fibre reinforced self-compacting concrete,” *Construction and Building Materials,* vol. 28, p. 287–293, 2012.

[17] H. Hu, P. Papastergiou, H. Angelakopoulos, M. Guadagnini and K. Pilakoutas, “Flexural performance of steel fibre reinforced concrete with manufactured and recycled steel fibres,” Zadar, 2017.

[18] A. Caggiano, H. Xargay, P. Folino and E. Martinelli, “Experimental and numerical characterization of the bond behavior of steel fibers recovered from waste tires embedded in cementitious matrices,” *Cement & Concrete Composites,* vol. 62, p. 146–155, 2015.

[19] O. Sengul, “Mechanical behavior of concretes containing waste steel fibers recovered from scrap tires,” *Construction and Building Materials,* vol. 122, pp. 649-658, 2016.

[20] W. Zhang, Y. Hama and S. H. Na, “Drying shrinkage and microstructure characteristics of mortar incorporating ground granulated blast furnace slag and shrinkage reducing admixture,” *Construction and Building Materials,* no. 93, pp. 267-277, 2015.

[21] K. Zdanowicz and S. Marx, “Shrinkage and Expansion Strains in Self-compacting Concrete Comparison of Methods of Measurements,” Maastricht, 2018.

[22] D. W. Hobbs, “Influence of Aggregate Restraint on the Shrinkage of Concrete,” *ACI Journal,* pp. 445-450, 1974.

[23] R. I. Gilbert, “Shrinkage, Cracking and Deflection the Serviceability of Concrete Structures,” *Electronic Journal of Structural Engineering,* vol. 1, pp. 15-37, 2001.

[24] M. Hoshino, “Relation Between Bleeding, Coarse Aggregate, and Specimen Height of Concrete,” *ACI Materials Journal,* vol. 86, no. 2, pp. 185-190, 1989.

[25] J.-H. Jeong, Y.-S. Park and Y.-H. Lee, “Variation of Shrinkage Strain within the Depth of Concrete Beams,” *Materials,* pp. 7780-7794, 2015.

[26] RILEM-TC-107-CSP, “RILEM TC 107-CSP: Creep and shrinkage prediction models: principles of

their formation," *Materials and structures,* vol. 31, pp. 507-512, 1998.

[27] A. Castel, S. J. Foster, T. Ng, J. G. Sanjayan and R. I. Gilbert, "Creep and drying shrinkage of a blended slag and low calcium fly ash geopolymer Concrete," *Materials and Structures,* vol. 49, no. 5, p. 1619–1628, 2016.

[28] A. M. Neville, Properties of Concrete, Fourth ed., London: Pearson Education Limited, 2004.

[29] I. Gilbert, "Concrol of cracking caused by restraint to early-age deformation," Dundee, 2016.

[30] M. Grzybowski and S. P. Shah, "Shrinkage Cracking of Fiber Reinforced Concrete," *ACI Materials Journal,* vol. 87, no. 2, pp. 138-148, 1990.

[31] H. Choi, M. Lim, R. Kitagaki, T. Noguchi and G. Kim, "Restrained shrinkage behavior of expansive mortar at early ages," *Construction and Building Materials,* vol. 84, p. 468–476, 2015.

[32] R. Bloom and A. Bentur, "Free and Restrained Shrinkage of Normal and High-Strength Concretes," *ACI Materials Journal,* vol. 92, no. 2, pp. 211-217, 1995.

[33] A. M. Paillere, M. Buil and J. J. Serrano, "Effect of Fiber Addition on the Autogenous Shrinkage of Silica Fume Concrete," *ACI Materials Journal,* vol. 86, no. 2, pp. 139-144, 1989.

[34] S. Altoubat and D. Lange, "Creep, shrinkage and cracking of restrained concrete at early age," *ACI Materials Journal,* vol. 98, no. 4, pp. 323-331, 2001.

[35] T. Aly and J. G. Sanjayan, "Shrinkage cracking properties of slag concretes with one-day curing," *Magazine of Concrete Research,* vol. 1, no. 60, pp. 41-48, 2008.

[36] A. Leemann, P. Lura and R. Loser, "Shrinkage and creep of SCC – The influence of paste volume and binder composition," *Construction and Building Materials,* vol. 25, no. 5, pp. 2283-2289, 2011.

[37] R. Loser and A. Leemann, "Shrinkage and restrained shrinkage cracking of self-compacting concrete compared to conventionally vibrated concrete," *Materials and Structures,* no. 42, pp. 71-82, 2009.

[38] EN-14651, "Test methods for metallic fibred concrete - Measuring the flexural tensile strength (limit of proportionality (LOP), residual)," European Committee for Standardization, Brussels, 2005.

[39] BSI-12, "Testing concrete - BS 1881 Part 119: Method for determination of compressive strength using portions of beams broken in flexure (equivalent cube method)," Board of BSI, London, 1998.

[40] H. Hu, P. Papastregiou, H. Angelakopoulas, M. Guadagnini and K. Pilakoutas, "Mechanical properties of SFRC Using blended manufactured and recycled tyre steel fibres," *Construction and Building Materials,* no. 163, pp. 376-389, 2018.

[41] CEN, "Eurocode 2: Design of concrete structures, Part 1-1: General rules and rules for Structures 2004," European Committee for Standardization, Brussels, 2008.

[42] fib, “fib Model Code for Concrete Structures 2010,” Wilhelm Ernst & Sohn, Berlin, Germany, 2013.

[43] L. Jianyong and Y. Yan, “A study on creep and drying shrinkage of high performance concrete,” *Cement and Concrete Research,* no. 31, pp. 1203-1206, 2001.

[44] W. Mitchell and C. Arya, “The effect of combining shrinkage-reducing-admixture with ground, granulated, blast-furnace slag on the drying shrinkage of concrete,” UCL Department of Civil, Environmental and Geomatic Engineering, London, 2015.

[45] Z. Al-Kamyani, M. Guadagnini and K. Pilakoutas, “Non-uniform drying shrinkage of RC elements with steel fibres,” Muscat, 2017.

[46] R. D. T. Filho, K. Ghavami, M. A. Sanjua´n and G. L. England, “Free, restrained and drying shrinkage of cement mortar composites reinforced with vegetable fibres,” *Cement & Concrete Composites,* vol. 27, no. 5, pp. 537-546, 2005.

[47] Z. P. Bazant and S. Baweja, “Creep and Shrinkage Prediction Model for Analysis and Design of Concrete Structures: Model B3,” ACI, Michigan, 2001.

[48] B. Craeye, G. D. Schutter, B. Desmet, J. Vantomme, G. Heirman, L. Vandewalle, Ö. Cizer, S. Aggoun and E. Kadri, “Effect of mineral filler type on autogenous shrinkage of self-compacting concrete,” *Cement and Concrete Research,* no. 40, p. 908–913, 2010.

[49] A. Leemann and P. Lura, “Creep and Shrinkage of SCC,” in *Mechanical Properties of Self-Compacting Concrete*, K. Khayat and G. (. De Schutter, Eds., Springer International Publishing, 2014, pp. 73-94.

[50] D. Snoeck, O. Jensen and N. D. Belie, “The influence of superabsorbent polymers on the autogenous shrinkage properties of cement pastes with supplementary cementitious materials,” *Cement and Concrete Research,* no. 74, pp. 59-67, 2015.

[51] M. Beddar, “An experimental study of porosity and premeability characteristics of steel fibre reinforced concrete,” in *Cement Combinations for Durable Concrete*, Dundee, 2005.

[52] ABAQUS, “Software Documentation, Version 6.14 SIMULIA,” Dassault Systèmes, RI, USA, 2014.

[53] C. A. Clear, “Cement type/early age properties,” Concrete Today, 2011.

[54] A. P. Fantilli, H. Mihashi and P. Vallini, “Multiple cracking and strain hardening in fiber-reinforced concrete under uniaxial tension,” *Cement and Concrete Research,* vol. 39, p. 1217–1229, 2009.

[55] K. Wille, S. El-Tawil and A. Naaman, “Properties of strain hardening ultra high performance fiber reinforced concrete (UHP-FRC) under direct tensile loading,” *Cement & Concrete Composites,* vol. 48, pp. 53-55, 2014.

[56] RILEM-TC-162-TDF, “RILEM TC 162-TDF: Test and design methods for steel fibre reinforced concrete,” *Materials and Structures,* vol. 36, pp. 560-567, 2003.